

1  
2  
3  
4  
5  
6  
7  
8  
9  
10  
11  
12  
13  
14  
15  
16  
17  
18  
19  
20  
21  
22  
23  
24

**South Atlantic Meridional Fluxes**

by

Silvia L. Garzoli<sup>1</sup>, Molly O. Baringer<sup>1</sup>, Shenfu Dong<sup>2,1</sup>,  
Renellys C. Perez<sup>2,1</sup>, and Qi Yao<sup>2,1</sup>

<sup>1</sup> Atlantic Oceanographic and Meteorological Laboratory, National Oceanographic and Atmospheric  
Administration (AOML, NOAA)

<sup>2</sup> Cooperative Institute for Marine and Atmospheric Studies (CIMAS), University of Miami

Submitted to Deep Sea Research  
June 2012

## Abstract

The properties of the meridional overturning circulation (MOC) and associated meridional heat transport (MHT) and salt fluxes are analyzed in the South Atlantic. The oceanographic data used for the study consist of Expendable bathythermograph (XBT) data collected along 27 sections at nominally 35°S for the period of time 2002 to 2011, and Argo profile data collected in the region. Previous estimates obtained with a shorter record are improved and extended, using new oceanographic sections and wind fields. Different wind products are analyzed to determine the uncertainty in the Ekman component of the MHT derived from their use. Results of the analysis provide a nine-year time series of MHT, and volume transport in the upper layer of the MOC. Salt fluxes at 35°S are estimated using a parameter introduced by numerical studies, the  $M_{ov}$  that represents the salt flux and helps determine the basin scale salt feedback associated with the MOC. Volume and heat transport by the western and eastern boundary currents are estimated, and their covariability is examined. Analysis of the data shows that the South Atlantic is responsible for a northward MHT with a mean value of  $0.54 \pm 0.14$  PW. The MHT exhibits no significant trend from 2002 to 2011. The MOC varies from 14.4 to 22.7 Sv with a mean value of  $18.1 \pm 2.3$  Sv and the maximum overturning transport is found at a mean depth of 1250 m. Statistical analysis suggests that an increase of 1 Sv in the MOC leads to an increase of the MHT of  $0.04 \pm 0.02$  PW. Estimates of the  $M_{ov}$  from data collected from three different kinds of observations, contrary to those obtained from models, feature a positive salt advection feedback ( $M_{ov} < 0$ ) suggesting that freshwater perturbations will be amplified and that the MOC is bistable. In other words, the MOC might collapse with a large enough freshwater perturbation. Observations indicate that the mean value of the Brazil Current is  $-8.6 \pm 4.1$  Sv at 24°S and  $-19.4 \pm 4.3$  Sv at 35°S, increasing towards the south. East of 3°E, the northward flowing Benguela Current and Agulhas rings have a net northward transport of  $22.5 \pm 4.7$  Sv. No significant correlation is observed between the MOC and the Brazil Current transport, and most of the compensation derives from the eastern boundary and interior transports. Products from the Ocean general circulation model For the Earth Simulator (OFES) are used to validate methodology used to extend the XBT record, and to aid in the interpretation of the observed findings.

## 1. Introduction

The mechanisms and pathways of mass and heat transport in the global ocean are due in large part to the wind-driven and buoyancy-driven components of the meridional overturning circulation (MOC). Associated with the strong thermohaline (buoyancy-driven) circulation in the Atlantic Ocean heat and salt are exchanged between the hemispheres. The South Atlantic Ocean plays a unique role in the global energy balance, transporting heat from the poles to the equator (e.g., Talley, 2003) as upper layer water spreads northward to compensate for the southward export of colder North Atlantic Deep Water. The northward flow is a complex mixture of waters originating from the Indian and Pacific oceans, blended together in the South Atlantic and overlain by large-scale gyre circulations. The ability to understand and quantify this northward flow is crucial to properly model and forecast weather and climate. Maximum northward heat transport is observed in the subtropical North Atlantic, 1.3 PW (1 PW =  $10^{15}$  Watts) accounting for 25% of the global combined atmosphere-ocean heat flux (e.g., Hall and Bryden, 1982; Lavin *et al.*, 1998; Ganachaud and Wunsch, 2003; Lumpkin and Speer, 2007; Johns *et al.*, 2011). Observed and simulated estimates of the meridional heat transport (MHT) in the South Atlantic range from negative values (-0.23 PW, de las Heras and Schlitzer, 1999) to almost 1 PW (0.94 PW, direct method, Saunders and King, 1995; 0.88 PW, Inverse model, Fu, 1981). The main reason for the large range in estimated MHT values for the South Atlantic is the limited amount of data available in the region at the time. The South Atlantic has been historically one of the least sampled basins, and as an expected consequence, model estimates in this region have been poorly constrained. In the past decade, however, the situation has been improved by the initiation of repeated high-density expendable bathythermograph (XBT) lines (AX18 crossing the South Atlantic from South America to South Africa, AX22 across Drake Passage, and AX25 across the Agulhas retroflexion), as well as the broad scale temperature and salinity profiles collected throughout the region by the Argo program (Roemmich and Owens, 2000) and the quasi-decadal occupation of several trans-basin hydrographic lines (e.g., Saunders and King, 1995; McDonagh and King, 2005; Bryden *et al.*, 2011).

Due to the above-described increase in data coverage in the South Atlantic, observed and simulated estimates of mean MHT and the MOC in the region have become more consistent. Baringer and Garzoli (2007) developed a methodology to obtain the heat transport from XBT data collected nominally along the latitude 35°S (XBT line AX18). Using this methodology, Garzoli and Baringer (2007) estimate the mean MHT from 14 AX18 sections, collected between July 2002 and May 2006, as 0.54 PW with a standard deviation of 0.11 PW. Using an extended version of the AX18 data set (17 sections collected between July 2002 and March 2007), Dong *et al.* (2009) estimate the mean strength of the meridional overturning circulation (MOC), defined as the maximum volume transport stream function (equivalent to the total northward transport in the upper water column), and the MHT. The obtained time-mean MOC is  $17.9 \pm 2.2$  Sv and MHT is  $0.55 \text{ PW} \pm 0.14 \text{ PW}$ . They show that MHT variability is significantly correlated with the MOC variability, where a 1 Sv increase in the strength of MOC would yield a  $0.05 \pm 0.01$  PW increase in the MHT. Dong *et al.* (2009) also partition the MOC and MHT into contributions from the western and eastern boundaries and the interior, and demonstrated that the variability of the contributions from boundary currents and interior are comparable.

Observations indicate that the annual cycle of the Ekman component of the flux is out of phase and of the same order of magnitude as the geostrophic component (Garzoli and Baringer, 2007; Dong *et al.*, 2009). As a consequence, the observed annual cycles of the total (Ekman plus geostrophic) MHT and the MOC are almost non-existent. Models, in contrast, show a strong annual cycle for the total MHT, as well as for the MOC, in the South Atlantic that depends very little on the geostrophic component of the fluxes (Jayne and Marotzke, 2001; Baringer and Garzoli, 2007; Dong *et al.*, 2011; Perez *et al.*, 2011). Therefore, the dominant variability arises from the Ekman component of the fluxes that has a marked seasonal cycle.

Another important concept for which observations and models are in disagreement is the direction of the salt flux within the Atlantic sector, which is an indicator for the stability of the overturning circulation (Dijkstra, 2007; Huisman *et al.*, 2010; Bryden *et al.*, 2011).

The stability and variability of the Atlantic MOC has been the object of numerous model studies (e.g., Weijer *et al.*, 2003; Weijer and Dijkstra, 2003). De Vries and Weber (2005) showed from modeling studies that the instability of the MOC results from salt feedback in the ocean. When the MOC transports salt to the North Atlantic, a decrease in the MOC due to a freshwater anomaly in the convection sites will amplify the fresh water anomaly further by freshening the Atlantic basin. In contrast, when the MOC transports freshwater to the north, a decrease in the MOC due to a freshwater anomaly in the convection sites will damp the freshwater anomaly by the salinification of the Atlantic basin. Drijfhout *et al.* (2011) reinforced this concept that the basin-scale MOC-salt feedback determines whether the thermohaline circulation is monostable or bistable and that a more robust estimate of the MOC-trend and its variability can be made by combining sections in the North and South Atlantic. The basin-scale MOC-salt feedback is associated with the sign of the overturning component of the fresh water flux, defined as the  $M_{ov}$ . According to Drijfhout *et al.* (2011) the sign of  $M_{ov}$  at the latitude 35°S in particular can be used to determine the stability of the MOC. In other words, when the  $M_{ov}$  in the South Atlantic is positive (negative salt advection feedback), salt is transmitted to the south and the MOC is monostable; when the  $M_{ov}$  is negative (positive salt advection feedback), salt is transmitted to the north and the MOC is bistable; it might collapse with a large enough freshwater perturbation.

The objectives of this paper are: to present new estimates of the MHT and MOC obtained by using a higher resolution wind field and the XBT data collected up to present (from July 2002 to February 2011); to provide an estimate of the  $M_{ov}$  from different kind of observations; and, to analyze the time series of volume transport to obtain estimates of the flows at the boundaries and the component of the MHT associated with them. Results are compared with estimates from a high-resolution eddy-resolving model, the Ocean general circulation model For the Earth Simulator (OFES) run by Japan Agency for Marine-Earth Science and Technology (JAMSTEC).

## 2. Methodology

The methodology used in this paper to obtain the MHT and MOC has been previously

described in Baringer and Garzoli (2007) and Dong *et al.* (2009). Baringer and Garzoli (2007) tested the methodology with previous full depth CTD data and model products, and concluded that it can provide heat transport estimates with a maximum uncertainty of  $\pm 0.18$  PW. The methodology can be summarized as follows: Salinity (S) is estimated for each XBT profile by using empirical relationships developed for the South Atlantic by Thacker (2008) from available Argo profiler and CTD data in the region to provide an estimate of S as a function of Temperature (T),  $T^2$ , pressure (p), latitude, and longitude. Where insufficient CTD and Argo data are available to define a statistically robust empirical estimate for S, the World Ocean Atlas 2001 (WOA01) gridded annual climatology (Stephens *et al.*, 2002) is used. XBT profiles provide data only up to about 850 m, and the data are extended to the bottom using the WOA01 gridded  $0.25^\circ$  climatology interpolated to the location of each XBT profile to generate an annual mean climatology for the deep ocean. The bottom is determined to be the depth at the location of the XBT profile from the Smith and Sandwell (1997) two-minute database of bathymetry. Note, although an updated version of the World Ocean Atlas was generated in 2009 (WOA09), the coarse resolution used for WOA09 ( $1^\circ$ ) does not resolve oceanic features at the eastern boundaries as well as WOA01. Hence, WOA01 is used in this study.

Ekman volume and heat transports are determined using a daily NCEP reanalysis (Kalnay *et al.*, 1996) winds interpolated to the location of the XBT observations. Observed temperatures from the XBT lines are used to determine the mixed layer depth and temperatures to compute the Ekman heat transport (Baringer and Garzoli, 2007). The net meridional volume and heat transport are then given by the sum of the geostrophic (described below) and Ekman components of the volume and heat transport.

Geostrophic velocities are determined from the T and S fields generated from XBT, CTD and Argo observations using the dynamic height method where an initial level of no motion is chosen at  $\sigma_2 = 37.09 \text{ kg m}^{-3}$  ( $\sigma_2$  defined as potential density relative to 2000 dbar). These geostrophic velocities are then zonally and vertically integrated to obtain the geostrophic volume transport. Note, the initial level of no motion velocity field is

uniformly adjusted so that the net salt transport across the section matches the salt flux through the Bering Straits ( $27.6 \times 10^6 \text{ kg s}^{-1}$ , [Coachman and Aagaard, 1988](#)). Typically, values of this velocity adjustment are small and range from  $10^{-4}$  to  $10^{-6} \text{ m s}^{-1}$  (Baringer and Garzoli, 2007). This correction ensures that mass transport is approximately conserved across each section (to less than 1 Sv) and only has a 0.01-0.02 PW impact on the meridional heat transport (Baringer and Garzoli, 2007; Dong *et al.*, 2009).

Additional corrections to the net transports are made when needed to account for barotropic motions and for XBT sections that failed to terminate at the 200 m isobath or shallower on each side of the South Atlantic. During the initial stages of the XBT program, data were not collected near the boundaries for some of the sections (July 2002, November 2002 and July 2004). In those cases, Garzoli and Baringer (2007) made estimates of the missing flow and a correction was applied. For all sections near  $35^\circ\text{S}$ , a bottom velocity of  $-0.04 \text{ m/sec}$  was applied in the region west of  $40^\circ\text{W}$  where the data indicates the presence of strong boundary current flows to account for the barotropic southward flow of the Brazil Current and Deep Western Boundary Current beneath (Garzoli and Baringer, 2007). The value was derived from Peterson's (1992) review of bottom velocity observations in the region of the Brazil Malvinas confluence that quoted an average of  $-0.04 \text{ m/s}$ . For the sections ending at  $24^\circ\text{S}$  (see Appendix) a value of  $-0.02 \text{ m/sec}$  is used. This value is obtained from analysis of the mean bottom velocities from the Parallel Ocean Climate Model (POCM) model and OFES, as well as observations from the Deep Basin Experiment (Hogg and Owens, 1999) and data collected by Weatherly and Kim (2000) at  $18^\circ\text{S}$ .

The studies conducted by Garzoli and Baringer (2007) and Dong *et al.* (2009) use monthly NCEP winds to estimate the Ekman volume and heat transports. In this paper, all sections presented in Garzoli and Baringer (2007) and Dong *et al.* (2009), as well as those collected since those studies, are analyzed using the higher temporal resolution NCEP daily fields. Small differences in the individual values for the MHT are observed between the calculations with the two different wind products, however, as it will be

shown in Section 3b, the mean values are similar and the differences are well within the estimated uncertainty.

The methodology used to determine the strength of the MOC from the XBT-derived volume transport was previously described in Dong *et al.* (2009). As in that study, the depth of the maximum cumulative volume transport, i.e., the depth where the meridional volume transport reverses direction from northward in the upper layer to southward in the lower layer, is computed. Then the strength of the MOC is simply defined as the maximum cumulative volume transport in the upper layer.

The model comparisons presented in this paper are made with fields obtained from the OFES model, an eddy-resolving model with a horizontal resolution of  $0.1^\circ$  and 54 vertical z-levels. The OFES simulation was spun up for 50-years with a monthly climatology derived from NCEP/NCAR reanalysis atmospheric fluxes (Masumoto *et al.*, 2004), and then forced with daily mean NCEP/NCAR reanalysis data from 1950 to 2007 (Sasaki *et al.*, 2008). Model fields were provided by JAMSTEC at  $0.2^\circ$  increments (every other horizontal grid point) in the entire South Atlantic region from 1980 to 2007, and also at the full model resolution ( $0.1^\circ$ ) along  $34.5^\circ\text{S}$  from 1980 to 2011 for direct comparisons of the mean during the XBT period (personal communication, Y. Sasai, 2011). Atmospheric fields used to force the model were provided by JAMSTEC at the full model resolution.

#### **a. The XBT observations**

The locations of the XBT lines are shown in Figure 1. The original AX18 XBT line was conducted from Cape Town to Buenos Aires, nominally along the latitude  $35^\circ\text{S}$  using Evergreen container ships. After the cruise conducted in March - April 2007, the shipping company eliminated that transect. Several attempts have and are still being made to routinely conduct these cruises along the original route. From October 2007 to June 2010, the route was from Cape Town to Santos or Rio (terminating near  $24^\circ\text{S}$  on the western boundary). For the purpose of the discussion in this paper these transects will be called AX18\*. Since June 2010, the transits have returned to the Cape Town to Buenos Aires

route. Further information on the data collected during each one of the lines can be obtained at [http://www.aoml.noaa.gov/phod/hdenxbt/ax\\_home.php](http://www.aoml.noaa.gov/phod/hdenxbt/ax_home.php).

In order to combine the observations collected along the two different transects, we adjusted the heat transport from AX18\* to AX18. This is done by assuming that the heat in the triangle formed by the two different lines (shown as solid black lines on Figure 1) is conserved. In other words, the heat transport difference between AX18 and AX18\* is balanced by the heat storage rate integrated over the triangle volume and surface heat exchange with the atmosphere integrated over the triangle area. Using Argo data to estimate the heat storage rate and monthly NCEP/NCAR air-sea heat flux data to estimate the net surface heat exchange with the atmosphere, the net heat transport across the XBT sections can be adjusted to account for the changing latitudes of AX18 and AX18\* (the methodology is described in detail in the Appendix). This correction varies seasonally and interannually and the amplitude of the seasonal cycle is approximately 0.2 PW with maximum in austral winter. As the result of this adjustment, a longer MHT time series that incorporates data collected both along AX18\* and AX18 lines, was made possible. Note, the OFES simulation is used to validate the adjustment methodology, and a similar seasonal cycle is produced albeit with a much weaker (0.1 PW) amplitude.

## **b. Winds**

The above described heat transport adjustment is needed because in this regions the winds vary significantly with latitude. The Ekman component of the meridional heat flux between 28°S and 38°S is computed using the monthly WOA01 temperatures for the mixed layer and the NCEP daily wind products for the period of the observations. Results are shown in the left panel of Figure 2. Large differences are observed between the wind fields along the new diagonal transect (AX18\*) from 24°S and the original transect nominally along 35°S (AX18).<sup>1</sup>

---

<sup>1</sup>Note, information on the wind stress fields during each of the AX18 and AX18\* cruises can be obtained at [http://www.aoml.noaa.gov/phod/hdenxbt/ax\\_home.php](http://www.aoml.noaa.gov/phod/hdenxbt/ax_home.php).<sup>1</sup>

The winds vary meridionally such that the mean Ekman heat transport changes from northward to southward as it moves northward from 35°S (Figure 2, right panel), changing sign in the mean at approximately 31°S. The amplitude of the seasonal cycle of the Ekman heat transport is much larger than the mean with amplitudes of about 0.2 PW. The amplitude of the seasonal cycle increases to the north of 38°S, reaching a maximum near 32°S and decreasing again north of 32°S (Figure 2, right panel). The Ekman heat transport has a maximum northward transport in austral winter (e.g., July) and a maximum southward transport in austral summer (e.g., Jan). The squares in the left panel of Figure 2 indicate the mean latitude of each of the XBT transects during the time of each section. The seven AX18\* cruises, located with mean latitude north of 30°S, were centered in typically negative (i.e., southward) Ekman heat transport, e.g., October 2007 through January 2010 (Figure 2, left panel); note, the July 2009 has a slightly positive Ekman heat transport consistent with the seasonal variability of the winds).

Given the importance of the contribution of the Ekman heat transport to the total MHT variability in the region, the sensitivity of the total MHT to the Ekman heat transport computed from several different wind products subsampled to the time and mean latitude of the XBT sections was evaluated. These wind products include: 1) Hellerman and Rosenstein (1983) monthly winds, 2) ECMWF monthly winds, 3) NCEP monthly winds (used by Baringer and Garzoli, 2007), and 4) monthly averages of NCEP daily winds (used in this study). Results are shown in Figure 3. There are differences between the Ekman heat transport estimates obtained from the monthly averages of the daily wind products from NCEP (red line in Figure 3) and those obtained with NCEP monthly winds (green line in Figure 3) of up to  $\pm 0.1$  PW that often exceed the differences between the Ekman heat transport derived from the different wind products (Hellerman, ECMWF, NCEP). Despite the sometimes-large instantaneous differences, the mean difference of the Ekman transport estimates based on the different data sets differ by less than 0.04 PW (0.062 PW to 0.1 PW).

### 3. Results

#### a. MHT

A time series of the MHT is generated from the data collected nominally at 35°S (Figure 4). The mean estimate of the MHT from the 27 realizations is 0.54 PW with a standard deviation of 0.14 PW. Note, that a similar mass conservation requirement rather than the salt conservation requirement applied here yields a mean heat transport of  $0.56 \pm 0.14$  PW. The observed variability is large, with values ranging from 0.30 PW to 0.82 PW, and despite the relatively small sample size no significant trend ( $-0.01 \pm 0.2$  per decade) is estimated from the 27 XBT sections.

Analysis of the variability of the different components of the MHT, the Ekman and geostrophic components, indicate that the annual cycle of the Ekman component varies with a similar magnitude but in the opposite direction to that of the geostrophic component (Figure 5, left panel). As a result, there is no significant annual cycle in the total MHT as shown in the right panel of Figure 5, consistent with the results from the first 17 AX18 transects (Dong *et al.*, 2009). Due to this weak seasonal cycle, removing the seasonal cycle did not alter the trend estimate reported above. Note, to determine the statistical significance of the annual cycle of the Ekman component of the MHT derived from the 27 realizations (blue line in Figure 5, left panel), a time series of the daily NCEP values for the period of the observations, was extracted at 35°S and the annual cycle estimated. The resulting seasonal cycle of the Ekman component (dashed blue line in Figure 5, left panel) agrees well with the subsampled seasonal cycle.

The lack of significant annual cycle in the MHT contradicts results from ocean models. In models the annual variability is dominated by the Ekman heat transport component, with a small contribution from the geostrophic component. A recent study by Dong *et al.* (2011) suggests that the lack of variability in the geostrophic transport in the models is likely related to the weak variability of the model temperature and salinity fields.

Despite this lack of variability in the simulated geostrophic transport, models are able to reproduce the observed mean MHT, and the high variability seen in the MHT series. For example, Perez *et al.* (2011) estimated the mean MHT at 34.5°S from two models, the POCM and OFES, for the time period 1986 to 1997 as 0.50 PW and 0.42 PW, respectively. Figure 6 shows the OFES MHT time series from 1980 to 2011; the mean MHT is 0.38 PW from 1980 to 2011, 0.38 PW from 1980 to 2007 (time period analyzed by Dong *et al.*, 2011), and 0.39 PW for 2002 to 2011 (the period of XBT observations). In other words, there is no-significant trend in the model from 1980 to 2011. However, there is a statistically significant (at 95%) increasing MHT trend in the first thirteen years of the OFES model ( $+0.09 \pm 0.02$  PW/decade), followed by a weaker but still statistically significant decreasing trend from 2002 to 2011 ( $-0.07 \pm 0.06$  PW/decade) which overlaps with the observations given the large uncertainty in the observed trend ( $-0.01 \pm 0.2$  PW/decade). Figure 6 also shows that the MHT variability is comparable to the observed variability, and ranges from -0.2 to 1.0 PW on time scales longer than 60 days.

## **b. MOC**

As mentioned before, Dong *et al.* (2009) found that the variability of the MOC estimated from AX18 transects is significantly correlated with the MHT variability ( $r = 0.76$ ), such that a 1 Sv increase in the MOC would yield a  $0.05 \pm 0.01$  PW increase in the MHT. A similar response (high correlation and linear regression with slope of approximately 0.05 PW/Sv) has been found in POCM and the OFES models along 34.5°S (Dong *et al.*, 2011; Perez *et al.*, 2011). The depth of the observed maximum cumulative transports range between 1000 – 1400 m depth with an average of 1250 m, a value that is slightly deeper than the 1100 m found in the North Atlantic (Cunningham *et al.*, 2007). The MOC estimated from the extended AX18 time series are shown in Figure 7. In this longer time series, the MOC varies from 14.4 to 22.7 Sv with a mean value of 18.1 Sv and a standard deviation of 2.3 Sv. These values are similar to the values previously obtained from inverse models and observations in the South Atlantic (e.g. Ganachaud, 2003; Lumpkin and Speer, 2007; Dong *et al.*, 2009; Bryden *et al.*, 2011).

The corresponding MHT values have been superimposed on the MOC values in Figure 7 to highlight their covariability. The correlation between the two variables for the extended AX18 data set is still high ( $r = 0.73$ ), although the MHT values appear to be more normally distributed than the MOC values (histograms not shown) with more positive excursions in the MOC time series than in the MHT time series. Linear regression of MHT onto the MOC indicates that an increase of 1 Sv in the MOC will lead to an increase of  $0.04 \pm 0.02$  PW in the MHT, a slightly lower value than the previous estimate (Dong *et al.*, 2009), but not statistically different from those previously obtained with the shorter data set.

### c. $M_{ov}$

The stability of the Atlantic MOC was further investigated by Drijfhout *et al.* (2011), under various climate scenarios, using the WCRP CMIP3 data set of coupled atmosphere-ocean models. Results indicate that most models feature a negative salt advection feedback ( $M_{ov} > 0$ ): freshwater perturbations are damped by this feedback, excluding the existence of a stable ‘off-state’ for the MOC. It is shown that the MOC exports salt in these models ( $M_{ov} > 0$ ), which stabilizes the MOC because the models have a reduced inflow of intermediate waters relative to thermocline waters. Hence, it is vital to accurately simulate the vertical distribution of water masses in order to capture the processes that can control MOC variability.

In this paper, the data collected nominally along 35°S is used to estimate the  $M_{ov}$ . The methodology used is the same as used by Drijfhout *et al.* (2011). The  $M_{ov}$  is defined as

$$M_{ov} = - \frac{1}{S_0} \int_{-\eta}^0 V^* \langle S \rangle dz \quad (1)$$

where  $S_0$  is the mean salinity of the section,  $V^*$  is the overturning component of the zonally integrated velocity across the section. By definition the vertical integral of  $V^*$  is zero.  $\langle S \rangle$  is the zonally averaged salinity (from the surface  $h$  to the bottom) that varies with depth.

The results from these calculations are shown as time series of  $M_{ov}$  in Figure 8. The  $M_{ov}$  values obtained varied from -0.28 to -0.05 Sv, with a mean value of -0.16 Sv. Additional values of the  $M_{ov}$  are obtained from CTD data collected along 30°S in the South Atlantic during two realizations of the A10 WOCE line and from a climatological section created from Argo data. Results are -0.15 Sv and -0.14 Sv for the cruises conducted during 1993 and 2003, respectively, and -0.11 Sv for the Argo climatological section. These independent  $M_{ov}$  estimates are within the range of variability of those obtained from the AX18 data and point to the robustness of the XBT-derived  $M_{ov}$  estimates. Note, the XBT-derived  $M_{ov}$  estimates are also in agreement with those recently calculated by Bryden *et al.* (2011): -0.09 Sv and -0.34 Sv from the WOCE CTD lines conducted along 24°S in 1983 and 2009, respectively. All of these  $M_{ov}$  estimates from the observations, contrary to the models, feature a positive salt advection feedback ( $M_{ov} < 0$ ) suggesting that freshwater perturbations will be amplified and that the MOC is bistable, it might collapse due to a large enough freshwater perturbation.

#### **d. Volume transport at the boundaries**

As mentioned in Section 2, in order to calculate the MOC and MHT, a self-consistent absolute velocity field was generated for each section. These velocity estimates can be further analyzed to determine the contribution of different currents to the observed variability. In particular on the western boundary, the southward volume transport in the upper layer (0 to 800 m) is associated with the Brazil Current. Between 23° to 24°S, historical data shows geostrophic transports of about -10 Sv (e.g. Stramma, 1989) in the Brazil Current. Further south, due to a recirculation cell found in the western South Atlantic south of 28°S, the transport associated with the Brazil Current increases and at 33°S is estimated to be -17.5 Sv (e.g. Stramma, 1989). Further south, at about 38°S, the Brazil Current volume transport reaches values as high as -22 Sv (e.g., Olson *et al.*, 1988; Peterson and Stramma, 1991; Garzoli, 1993).

Garzoli and Baringer (2007) previously estimated from the XBT data that the transports of the Brazil Current at 35°S range from -25 to -12 Sv with a mean of -19 Sv. From the extended XBT series, a nine year-long term time series of Brazil Current is constructed. (Figure 9, left panel). The mean Brazil Current volume transport for the 18 cruises along the original AX18 line (17 cruises before October 2007 and the October 2009 cruise) crossing the Brazil Current at nominally 35°S is  $-19.4 \pm 4.3$  Sv. The Brazil Current volume transport for the 9 cruises along the AX18\* line (crossing the Brazil Current at nominally 24°S) is  $-8.6 \pm 4.1$  Sv. These results confirm the existence of a weaker Brazil Current north of 28°S, whose volume transport is increased by a recirculation cell south of that latitude. In comparison, the OFES model has a Brazil Current at 35°S of  $-21 \pm 4.7$  Sv, a value that is very similar to the one obtained from the observations.

On the eastern boundary, the mean volume flow is mostly associated to the upper limb of the MOC that enters the Atlantic as the Agulhas leakage. At 35°S and east of the Walvis ridge (east of 3°E) this flow has two components: the Benguela Current, which has a well-defined mean flow that is mostly confined near the continent, and a more variable transient flow mostly on the western side, east of 10°E. This transient flow is dominated by large rings shed from the Agulhas Retroflexion (e.g. Peterson and Stramma, 1991; Stramma and England, 1999; de Ruijter *et al.*, 1999, Richardson and Garzoli, 2003, Baker-Yeboah *et al.*, 2010, Beal *et al.*, 2011). The integrated volume transport from the South African coast to 3°E mostly represents the steady component of the Benguela Current (Garzoli and Gordon, 1996; Richardson and Garzoli, 2003). Results of the BEST experiment (Garzoli and Gordon, 1996) indicated that the northward transport of the Benguela Current at 30°S is 16 Sv. Other reports of Benguela Current transport range from around 15 to 25 Sv (Stramma and Peterson, 1989; Gordon *et al.*, 1992; Sloyan and Rintoul, 2001). Differences in transport estimates are probably due to fluctuations of the currents, and the variability associated with the Agulhas rings and methodology differences.

From the extended XBT time series, the mean volume transport east of 3°E is 22.5 Sv with a standard deviation of 4.7 Sv (Figure 9). The average volume transport obtained

from data collected along AX18 is 23.2 Sv with a standard deviation of 4.4 Sv. Similar estimates obtained from data collected along AX18\* are 21.3 Sv with a standard deviation of 5.2 Sv. In comparison, the OFES model has a northward flow east of 3°E of  $16.2 \pm 3.5$  Sv. Those results from XBT and OFES model are consistent with estimates from previous studies.

A very high correlation is observed between the volume transport and heat transport from the surface to 800 m. It must be noted that for the boundary currents, the temperature/heat transport is calculated from the surface to the bottom and integrated across the basin and in this case mass is conserved. The temperature/heat transport values of the major ocean currents quoted herein are from the mass-balanced circulation, but are computed above 800 m depth. While these may be considered temperature transports, we use the term heat transport to remind the reader that the values of the currents are derived from the mass-balanced circulation. The volume and heat transport correlation for the Brazil Current is 0.95 and for the Benguela Current is 0.91 (Figure 10). The regression between the variables indicate that in both cases an increase in volume transport in the upper 800 m of 1 Sv results in an increase of heat transport in the upper 800 m of  $0.06 \pm 0.01$  PW for the Brazil current and  $0.05 \pm 0.01$  PW for the Benguela Current.

#### **4. Summary and Conclusions**

In this paper, estimates of the MHT and the MOC obtained from data collected along the XBT transect nominally conducted at 35°S are extended by four years to cover the period 2002 to 2011. Estimates are improved using high-resolution wind fields and an improved hydrographic climatology. Results of the analysis provide a nine-year time series of MHT. This time series is made possible through an adjustment process where the net heat transport can be adjusted to account for the changing latitudes of the AX18 (Buenos Aires to Cape Town) and AX18\* (Santos or Rio to Cape Town) lines, using Argo data to estimate the heat storage changes in the triangle bounded by AX18 and AX18\* and NCEP air-sea flux products to estimate the net surface heat flux in that region. This adjustment varies seasonally and interannually, and the amplitude of the seasonal cycle is

approximately 0.2 PW with maximum in austral winter. Products from the OFES simulation are used to validate the methodology. Although the seasonal cycle of the OFES correction term is similar in phasing to the observed, the amplitude is much weaker (0.1 PW), the model demonstrates the skill of the adjustment procedure. Analysis of the sensitivity of the Ekman component of the heat transport to different wind products indicates that despite the sometimes large instantaneous differences, the mean difference of the Ekman transport estimates based on the different wind products differ by less than 0.04 PW (0.062 PW to 0.1 PW).

Estimates of MHT and MOC are close to those obtained during the first years of the experiment (2002 to 2007); however, the new analysis demonstrates the robustness of those earlier estimates and decreases the level of uncertainty. Estimates of the MHT obtained from data collected during the 27 transects conducted between 2002 to 2011 yield a mean value  $0.54 \pm 0.14$  PW. Despite the relatively small sample size, no significant trend ( $-0.01 \pm 0.2$  PW per decade) is estimated from the observations for the period of time 2002 to 2011. The new estimates for the MOC vary from 14.4 to 22.7 Sv with a mean value of  $18.1 \pm 2.3$  Sv. The MOC reaches this mean maximum value at a mean depth that is deeper than the corresponding mean depths in the North Atlantic (mean depth of 1250 m).

The MHT and MOC values are consistent with previous estimates obtained by models and observations in the South Atlantic in the latitude band 30°S to 35°S. They are also consistent with observations collected further north in the South Atlantic. Using data from two transatlantic hydrographic section along 24°S in 1983 and 2009, Bryden *et al.* (2011) estimate the MOC to be 16.5 Sv (1983) and 21.5 Sv (2009) and the corresponding values for the MHT are 0.4 PW (1983) and 0.7 PW (2009) respectively.

The stability of the MOC is assessed through the estimation of the meridional fresh water flux  $M_{ov}$ , that at 35°S determines the basin scale MOC salt feedback. Results obtained independently in this study from XBT sections, CTD casts, and Argo data agree well with previously published values (Bryden *et al.*, 2011). The observations consistently show

that the  $M_{ov}$  is negative (i.e., positive salt advection feedback) with a mean value from the XBT observations of  $-0.16$  Sv, whereas the models indicate a positive value for the  $M_{ov}$  (i.e., negative salt advection feedback). The observed negative values of the  $M_{ov}$  indicate that salt is transmitted to the north and the MOC is bistable; in other words, the MOC might collapse due to a large enough freshwater perturbation (Drijhout *et al.*, 2011).

Estimates of the boundary current volume transports in the upper layer confirm previous results that the Brazil Current increases its volume as it flows southward. Observations indicate that the mean value of the Brazil Current is  $-8.6 \pm 4.1$  Sv at  $24^\circ\text{S}$  and  $-19.4 \pm 4.3$  Sv at  $35^\circ\text{S}$ . East of  $3^\circ\text{S}$  the mean transport, the result of the northward flowing Benguela Current and Agulhas rings is  $22.5 \text{ Sv} \pm 4.7 \text{ Sv}$ . A very high correlation and linear relationship is observed between the volume transport and heat transport for the boundary currents (defined here as the integral from the surface to 800 m) indicating that an increase in volume transport of 1 Sv results in an increase of heat transport of  $0.06 \pm 0.01$  PW for the Brazil Current and  $0.05 \pm 0.01$  PW for the Benguela Current. In the Bryden *et al.*, (2011) study based on data collected during two research cruises, the observed difference between the MOC transports from those cruises are assumed to be primarily due to the different strength of the southward Brazil Current transport during the occupation of the sections: 12.2 Sv (1983) compared with 4.9 Sv (2009). The analysis of the data presented in this paper show no significant correlation between transports of the Brazil Current and the strength of the MOC ( $r = 0.09$ ), suggesting that the Brazil Current is compensated by transport in other regions. This hypothesis is supported by the analysis performed by Dong *et al.* (2009) where the contribution to the AMOC is divided among western boundary, interior and eastern boundary. Results from Dong *et al.* (2009) indicate that most of the western boundary transport compensation derives from the interior and the eastern boundary transports. Here, the correlation between the transports on the western and eastern boundary is modest but significant (approximately 0.4) indicating that the interior and the deep ocean also play an important role.

This extensive observational study points to important differences between observations and models, like the absence of a seasonal cycle in the observed MHT and the MOC, and

the difference in the sign of the  $M_{ov}$ . Further theoretical and modeling studies are required to explore the possible physical mechanisms responsible for these differences.

## **Appendix**

### **Adjusting the XBT observations**

In order to compare the estimates of the MHT obtained from data collected from both transects (the new AX18\* line and the original AX18 line), the heat balance in the triangle formed by the two different lines (Figure 1) is examined to estimate the heat transport adjustment required to convert transports across AX18\* to transports across AX18. That is to say how much heat is gained or lost in the triangle formed by the two different transects. The heat transport difference between AX18 and AX18\* can be estimated as the difference between the heat storage rate integrated over the triangle volume, and the air-sea heat exchange integrated over the triangle area. The heat storage rate is computed using the monthly gridded temperature data from Argo float profiles, which are produced by the Scripps Institution of Oceanography (Roemmich and Gilson, 2009). The air-sea heat fluxes are from the monthly NCEP/NCAR Reanalysis. Both quantities, the air-sea heat flux and the heat storage rate have a roughly equal magnitude, and show a marked annual cycle with a slight phase shift in austral winter (Figure A1, left). The annual cycles are derived from observations during the period 2002-2010. The maximum heat storage rate is observed in December (0.20 PW) and the minimum value is found in May (-0.22 PW). The air-sea heat flux has a maximum value during December (0.33 PW) and a minimum value during June (-0.40 PW). The heat transport divergence/convergence within the box defined by the AX18 and AX18\* sections varies by about  $\pm 0.2$  PW with the maximum during austral winter and a minimum in austral summer. This convergence/divergence estimate can be used to adjust the observed heat transport values along AX18\* so that they can be compared in a time series sense to the transports along AX18.

A similar analysis of the OFES fields from 2002 to 2007 was conducted to verify the validity of the procedure used to normalize the observations. Namely, the heat flux

correction was replicated using the same procedure used for the observations as described above. The seasonally averaged heat budget is shown in Figure A1 (right). The seasonal cycle of the MHT correction term is similar in phasing to the observed, with maximum in austral winter. However, the amplitude is much weaker ( $\pm 0.1$  PW compared with  $\pm 0.2$  PW). Interestingly, amplitude of the heat storage rate annual cycle in the model is nearly twice as large as that seen in observations ( $\pm 0.2$  PW for observations vs.  $\pm 0.35$  PW for the model). The net surface heat flux annual cycle is only slightly larger than that found in the NCEP model and is not enough to account for the discrepancy. The model appears to under represent the seasonal variability of ocean heat transport between these two lines; in other words in the model the ocean appears to be passively responding to air-sea forcing, without any seasonally varying currents to alter the heat transport between the two sections.

The model provides all terms for the heat budget instantaneously so that the difference between heat transports along AX18 and AX18\* should be by definition exactly equal to the difference of the heat content change and surface heat flux within the box. The degree to which the adjustment procedure reproduces the actual heat transport along AX18 given only the heat transport along AX18\* was tested within the context of the model (not shown). When the adjustment procedure described above is applied to the model heat transport, the mean difference between the MHT corrected and un-corrected along AX18\* decreases from 0.05 to 0.03 PW (0.46 PW compared with 0.42 PW), the standard deviation of the difference decreases from 0.15 to 0.10 PW, and the correlation increases from 0.74 to 0.93 for time scales longer than 60 days (not shown).

As can be seen in Figure A1 (top left) the AX18\* heat transport adjustment has a seasonal cycle that has a maximum positive adjustment in austral winter (e.g. July), that is in phase with the Ekman transport variability. Generally, when the seasonally varying Ekman heat transport is negative, the difference between the ocean heat storage rate and the heat gained from the atmosphere is also negative and the MHT adjustment is negative. However, the MHT adjustment can also vary interannually, and for the transect conducted during July 2009 the Ekman flow is slightly positive, and the difference

between the ocean heat storage rate and the heat gained from the atmosphere is positive and the MHT correction is positive. The seasonally aliased occupations of the AX18\* line, thus make the Ekman transport to appear particularly unusual along the new section, despite the fact that the mean Ekman heat transport changes only from about +0.1 PW to -0.03 PW between AX18 and AX18\*. The fact that the correction has a similar seasonal phase as the Ekman transports themselves is in part because the Ekman transports themselves have a larger seasonal amplitude along AX18 than AX18\* and the correction has the effect of increasing the seasonal cycle of the time series along AX18\*.

A time series of the MHT is generated from the data collected along AX18 and AX18\*, the latter adjusted using the correction explained previously. Figure A2 shows the temporal evolution of the total MHT nominally at 35°S (from AX18 and AX18\*) after the adjustment is applied (black line), as well as the geostrophic (red line) and the Ekman (blue) components. The green dots shown in Figure A1 are the total MHT obtained from the AX18\* route before the adjustment is applied. Note that the cruises conducted since June 2010 use the original AX18 ports and no correction was applied for these cruises. Figure A2 clearly shows the difference in the Ekman component of the MHT estimated from the data collected along AX18 and those from data along the AX18\* line. When the transect is conducted along AX18\*, in a region of mostly negative wind stress and hence negative Ekman transport (Figure 2, right panel), the Ekman component is typically negative (blue line in Figure A2 during the period 2007 to 2009). The variability of the winds with latitude and the consequent variability in the Ekman transport is one of the main reasons why it is needed to adjust the heat balance between the two different tracks.

## **Acknowledgements**

The authors would like to acknowledge Robert Roddy for taking care of the organization of the cruises and the instrumentation of the ships. Thanks also to our colleagues and collaborators from the National Hydrographic Service in Argentina for their support to the program. The authors would like also to acknowledge all of the ship riders that collected the XBT data: Lt. Cdr. Ariel Herman Triosi, Cdr. Fabian Vetere, Adrian Webb,

Walter L. Reynoso-Peralta, and Fergus McKay. Thanks to Carlos Garcia from the University of Rio Grande, Brazil and Lt. Vlatimir and Ct Marcelo Calvacante from the Brazilian Navy for their support of data collection during two of their cruises and, to all the captains and crews of the ships that supported the program. Thanks to Dr. Chris Meinen for helpful suggestions to the paper. XBT and Argo data collection and analysis are supported by grants from the Climate Observation Division, NOAA Climate Program Office.

## References

- Baringer, M. O., Garzoli S. L., 2007. Meridional Heat Transport determined with Expendable Bathythermographs. Part 1: Error estimates. *Deep-Sea Res., I*, doi:10.1016/j.dsr.2007.03.011.
- Baker-Yeboah, S., Byrne D. A., Watts D. R., 2010. Observations of Mesoscale Eddies in the South Atlantic Cape Basin: Baroclinic and Deep Barotropic Eddy Variability, *J. Geophys. Res.*, 115, 2010, doi:10.1029/2010JC006236.
- Beal, L. M., Wilhelmus P., De Ruijter M., Biastoch A., Zahn R., 2011. On the role of the Agulhas system in ocean circulation and climate. *Nature*, 472, 429–436 doi:10.1038/nature09983.
- Bryden, H. L., King B. A., McCarthy G. D., 2011. South Atlantic overturning circulation at 24°S. *J. Mar. Res.*, 69 (1), 38-55.
- Coachman, L.K., Aagaard, K., 1988. Transports through Bering Strait: annual and interannual variability. *J. Geophys. Res.*, 93, 15535–15539.
- Cunningham, S.A., Kanzow T., Rayner D., Baringer M.O., Johns W.E., Marotzke J., Longworth, H. R., Grant, E. M., Hirschi J.J-M., Beal, L. M., Meinen, C. S., Bryden, H. L., 2007. Temporal variability of the Atlantic meridional overturning circulation at 26.5°N. *Science*, 317, 935 – 938, doi:10.1126/science.1141304.
- de las Heras, M.M., Schlitzer, R., 1999. On the importance of intermediate water flows for the global ocean overturning. *J. Geophys. Res.* 104, 15515–15536.
- de Vries P., Weber S. L., 2005. The Atlantic freshwater budget as a diagnostic for the existence of a stable shut down of the meridional overturning circulation. *Geophys. Res. Lett.* 32. doi: 10.1029/2004GL021450
- De Ruijter, W. P. M., Biastoch, A., Drijfhout, S.S., Lutjeharms, J.R.E., Matano, R.P., Pichevin, T., Van Leeuwen, P.J., Weijer, W., 1999. Indian–Atlantic inter- ocean

exchange: Dynamics, estimation and impact. *J. Geophys. Res.* 104, 20885–20910.

Dong, S., Garzoli S., Baringer M., Meinen C., Goni G., 2009. Interannual variations in the Atlantic meridional overturning circulation and its relationship with the net northward heat transport in the South Atlantic. *Geophys. Res. Lett.*, 36, L20606, doi:10.1029/2009GL039356.

Dong, S., Garzoli S., Baringer M., 2011. The role of interocean exchanges on decadal variations of the meridional heat transport in the South Atlantic. *J. Phys. Oceanogr.*, 41, 1498–1511, doi: 10.1175/2011JPO4549.1.

Dijkstra, H. A., 2007. Characterization of the multiple equilibria regime in a global ocean model. *Tellus*, 59, 695–705.

Drijfhout, S.S., Weber, S. L., van der Waluw, E., 2011. The stability of the MOC as diagnosed from model projections for pre-industrial, present and future climates *Clim. Dyn.*, 37, 1575–1586, doi:10.1007/s00382-010-0930-z.

Fu, L. L., 1981. The general circulation and meridional heat transport of the subtropical South Atlantic determined by inverse methods. *J. Phys. Oceanogr.*, 11, 1171–1193.

Garzoli, S. L., 1993. Geostrophic velocities and transport variability in the Brazil/Malvinas Confluence. *Deep-Sea Res.*, 40, 1379–1403.

Garzoli, S. L., Baringer, M. O., 2007. Meridional heat transport determined with expendable bathythermographs, Part II: South Atlantic transport. *Deep-Sea Res.*, 54(8), 1402–1420.

Garzoli, S. L., Gordon, A. L., 1996. Origins and variability of the Benguela Current. *J. Geophys. Res.*, 101, 897–906.

Ganachaud, A. S. and Wunsch, C., 2003. Large-scale ocean heat and freshwater transports during the World Ocean Circulation Experiment. *J. Climate*, 16, 696–705.

Gordon, A. L., Weiss, R. F., Smethie, W. M., Warner, M. J., 1992. Thermocline and intermediate water communication between the South-Atlantic and Indian Oceans. *J. Geophys. Res. Oceans*, 97, 7223–7240.

Hall, M. M., Bryden, H. L., 1982. Direct estimates and mechanisms of ocean heat transport. *Deep-Sea Res.*, 29, 339–359.

Hellerman, S. and Rosenstein, M., 1983. Normal monthly wind stress over the World Ocean with error estimates. *J. Phys. Oceanogr.*, 13, 1093–1104.

Hogg, N. G. and Owens, W. B., 1999. Direct measurement of the deep circulation within the Brazil Basin. *Deep-Sea Res.* II, 46, 335–353.

- Huisman, S. E., den Toom, M., Dijkstra, H.A., Drijfhout, S.S., 2010. An indicator of the multiple equilibria regime of the Atlantic Meridional Overturning Circulation, *J. Phys. Oceanogr.*, 40, 551-567, doi:10.1175/2009JPO4215.1.
- Jayne, S. R., Marotzke, J. 2001. The dynamics of ocean heat transport variability. *Rev. Geophys.*, 39, 385-411.
- Johns, W.E., Baringer, M. O., Beal, L. M., Cunningham, S.A. , Kanzow, T., Bryden, H. L., Hirschi, J., Marotzke, J., Meinen, C., Shaw, B., and Curry, R., 2011. Continuous, array-based estimates of Atlantic Ocean heat transport at 26.5°N. *J. Climate*, 24(10):2429-2449.
- Kalnay, E., Kanamitsu, M., Kistler, R., Collins, W., Deaven, D., Gandin, L., Iredell, M., Saha, S., White, G., Woollen, J., Zhu, Y., Chelliah, M., Ebisuzaki, W., Higgins, W., Janowiak, J., Mo, K. C., Ropelewski, C., Wang, J., Leetmaa, A., Reynolds, R., Jenne, R., Joseph, D., 1996. The NCEP/NCAR 40-year reanalysis project, *Bull. Amer. Meteor. Soc.*, 77, 437-470.
- Lavin, A., Bryden, H. L., Parrilla, G., 1998. Meridional transport and heat flux variations in the subtropical North Atlantic. *Global Atmos. Ocean Syst.*, 6, 269-293.
- Lumpkin, R., Speer, K., 2007. Global Ocean Meridional Overturning. *J. Phys. Oceanogr.*, 37, 2550-2562.
- Masumoto, Y., Sasaki, H., Kagimoto, T., Komori, N., Ishida, A., Sasai, Y., Miyama, T., Motoi, T., Mitsudera, H., Takahashi, K., Sakuma, H., Yamagata, T., 2004. A fifty-year eddy-resolving simulation of the world ocean - preliminary outcomes of OFES (OGCM for the Earth Simulator). *J. Earth Simulator*, 1, 35-56.
- McDonagh, E. L. and King, B. A. (2005). "Oceanic fluxes in the South Atlantic." *J. Phys. Oceanogr.* 35(1): 109-122.
- Olson, D. B., Podesta, G. P., Evans R. H., Brown, O. B., 1988. Temporal variations in the separation of Brazil and Malvinas currents. *Deep-Sea Res.*, 35, 1971-1990.
- Perez, R. C., Garzoli, S. L., Meinen, C. S., Matano, R. P., 2011. Geostrophic velocity measurement techniques for the meridional overturning circulation and meridional heat transport in the South Atlantic. *J. Atmos. Oceanic Technol.*, 28, 1504-1521, doi: 10.1175/JTECH-D-11-00058.1.
- Peterson, R. G., Stramma, L., 1991. Upper-level circulation in the South Atlantic Ocean. *Prog. Oceanogr.* 26, 1-73.
- Peterson, R.G., 1992: The boundary currents in the western Argentine Basin. *Deep-Sea Research*, 39, 623-644.

775 Richardson, P. L., Garzoli, S. L., 2003. Characteristics of Intermediate Water Flow in the  
 776 Benguela Current as measured with RAFOS floats. *Deep-Sea Res.*, 50, 87-118.  
 777  
 778 Roemmich, D. and Gilson, J., 2009. The 2004-2008 mean and annual cycle of  
 779 temperature, salinity, and steric height in the global ocean from the Argo Program. *Prog.*  
 780 *Oceanogr.*, 82, 81-100.  
 781  
 782 Roemmich, D., Owens, W. B., 2000. The Argo Project: Global ocean observations  
 783 for understanding and prediction of climate variability. *Oceanogr.*, 13(2), 45-50.  
 784  
 785 Saunders, P. M., King, B. A., 1995. Oceanic fluxes on the WOCE A11 section. *J. Phys.*  
 786 *Oceanogr.*, 25, 1942–1958.  
 787  
 788 Sasaki, H., Nonaka, M., Sasai, Y., Uehara, H., Sakuma, H., 2008. An eddy-resolving  
 789 hindcast simulation of the quasiglobal ocean from 1950 to 2003 on the Earth Simulator.  
 790 High resolution numerical modelling of the atmosphere and ocean, K. Hamilton and W.  
 791 Ohfuchi, Eds., Springer, New York, 157-185.  
  
 792 Sloyan, B.M. and Rintoul, S.R., 2001. The Southern Ocean limb of the global deep  
 793 overturning circulation. *J. Phys. Oceanogr.*, 31, 143–173.  
  
 794 Smith, W. H. F., Sandwell, D. T., 1997. Global seafloor topography from satellite  
 795 altimetry and ship depth soundings. *Science*, 277, 195-196.  
 796  
 797 Stephens, C., Antonov, J. I., Boyer, T. P., Conkright, M. E., Locarnini, R., O'Brien T. D.,  
 798 2002. World Ocean Atlas 2001 Volume 1: Temperature [CD-ROM], edited by S. Levitus,  
 799 NOAA Atlas NESDIS 49, U.S. Govt. Printing Office, Washington, D. C.  
 800  
 801 Stramma, L., 1989. The Brazil current transport south of 23°S. *Deep-Sea Res.*, Part A, 36,  
 802 639-646.  
 803  
 804 Stramma, L., England, M., 1999. On the water masses and mean circulation of the South  
 805 Atlantic Ocean. *J. Geophys. Res.*, 104, 20863–20883.  
 806  
 807 Stramma, L., Peterson, R. G., 1989. Geostrophic transport in the Benguela current region.  
 808 *J. Phys. Oceanogr.*, 19, 1440–1448.  
 809  
 810 Talley, L. D., 2003. Shallow, intermediate and deep overturning components of the  
 811 global heat budget. *J. Phys. Oceanogr.*, 33, 530–560.  
  
 812 Thacker, W.C., 2008. Estimating Salinity between 25° and 45°S in the Atlantic Ocean  
 813 Using Local Regression. *J. Atmos. Oceanic Technol.*, 25, 114-130.  
  
 814 Weatherly, G. L., Y.Y. Kim, E. Kontar, 2000. Eulerian measurements of the North  
 815 Atlantic Deep Water Deep Western Boundary Current at 18°S. *J. Phys. Oceanogr.*, 30,  
 816 971-986.

817 Weijer, W., Dijkstra, H. A., Oksuzoglu, H. F., Wubs, W., de Niet, A. C., 2003. A fully-  
818 implicit model of the global ocean circulation. J. Comput. Phys., 192, 452-470.

819 Weijer, W., Dijkstra, H. A., 2003. Multiple oscillatory modes of the global ocean  
820 circulation. J. Phys. Oceanogr., 33, 2197-2213.  
821  
822

## List of Figures:

**Figure 1:** Locations of the high-density XBT lines conducted in the South Atlantic (all track lines shown in grey; typical AX18 and AX18\* track lines as described in text are shown in black). Blue shading indicates seafloor topography and the thin black line marks the 1,000 m isobath.

**Figure 2:** (left) Contoured monthly Ekman heat transport in PW derived from daily wind stress values with yellow squares highlighting the time and the mean latitude for the AX18 and AX18\* transects. (right) The mean value of the Ekman heat transport are shown at the right (solid black line) and the amplitude of the seasonal cycle (dashed blue line) as a function of latitude. The Ekman component of the meridional heat flux between  $38^{\circ}\text{S}$  and  $28^{\circ}\text{S}$  was computed using the monthly WOA01 temperatures to determine the mixed layer temperature and NCEP daily wind products.

**Figure 3:** Ekman heat transport as a function of time obtained for the following wind products: 1) Hellerman and Rosenstein (1983) (1983) monthly winds (blue line), 2) ECMWF monthly winds (pink), 3) NCEP monthly winds (used by Baringer and Garzoli, 2007) (green), and 4) monthly values obtained from the NCEP daily winds (red, this paper) corresponding to the XBT transect dates. Note that the Ekman transport values are computed directly along each XBT section that vary in latitude.

**Figure 4:** Meridional heat transport estimates as a function of time (black dots and line). Superimposed (red curve) is the 183-day running mean of the daily data obtained from linear interpolation of the black curve.

**Figure 5:** Left: Ekman (blue dots) and geostrophic (red dots) components of the MHT estimated from AX18 transects as a function of year-day, with the least-squares fit annual cycle overlaid. The blue dashed line is the annual cycle of the Ekman component of the flux obtained from the original daily NCEP data. Right: Total MHT from AX18 transects as a function of year-day.

**Figure 6:** MHT along 34.5°S as a function of time estimated from OFES (solid black line) for time scales longer than 60-days. The linear regressions from 1980-1993 and 2002-2010 are shown as red lines. The observed MHT time series along the nominal latitude is overlaid as yellow circles.

**Figure 7:** Time series of the MHT (black) and the AMOC (red) along nominally 35°S for the time period 2002 to 2011.

**Figure 8:** Time series of the  $M_{ov}$  nominally across 35°S for the time period 2002 to 2011.

**Figure 9:** Left panel: Volume transport of the Brazil Current at 35°S (red crosses in open circles) and 24°S (red dots) and the volume transport east of 3°E for cruises along 35°S (green crosses in open circles) and those along the diagonal cruises ending near 24°S (green dots). Right panel: the equivalent temperature/heat transports for the Brazil Current and currents east of 3°E.

**Figure 10:** Correlation between heat and volume transport for the Brazil Current (left, green dots) and for the flow between 3°E and the African coast (right, red dots) at nominally 35°S. The green and red line is the linear relation between the variables in those two regions, respectively.

**Figure A1:** Heat adjustment from AX18\* transect to AX18 transect obtained as the difference between the ocean heat storage rate and the heat gained from the atmosphere (within the box highlighted in Fig. 1): Annual cycle of the heat storage rate (green circles), air sea heat flux (red circles), and the heat transport adjustment (black circles) computed from the observations (left) and OFES (right).

**Figure A2:** MHT as a function of time estimated from AX18 transects (solid black line). The geostrophic and Ekman components of the MHT are shown in red and blue, respectively. Green dots show the unadjusted values collected along AX18\* (see text).

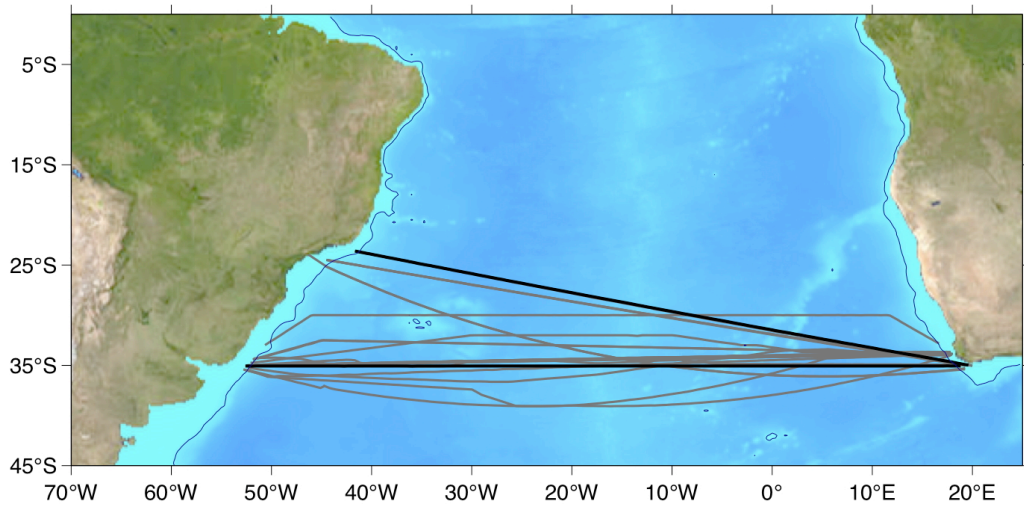


**Figure 1:** Locations of the high-density XBT lines conducted in the South Atlantic (all track lines shown in grey; typical AX18 and AX18\* track lines as described in text are shown in black). Blue shading indicates seafloor topography and the thin black line marks the 1,000 m depth topography.

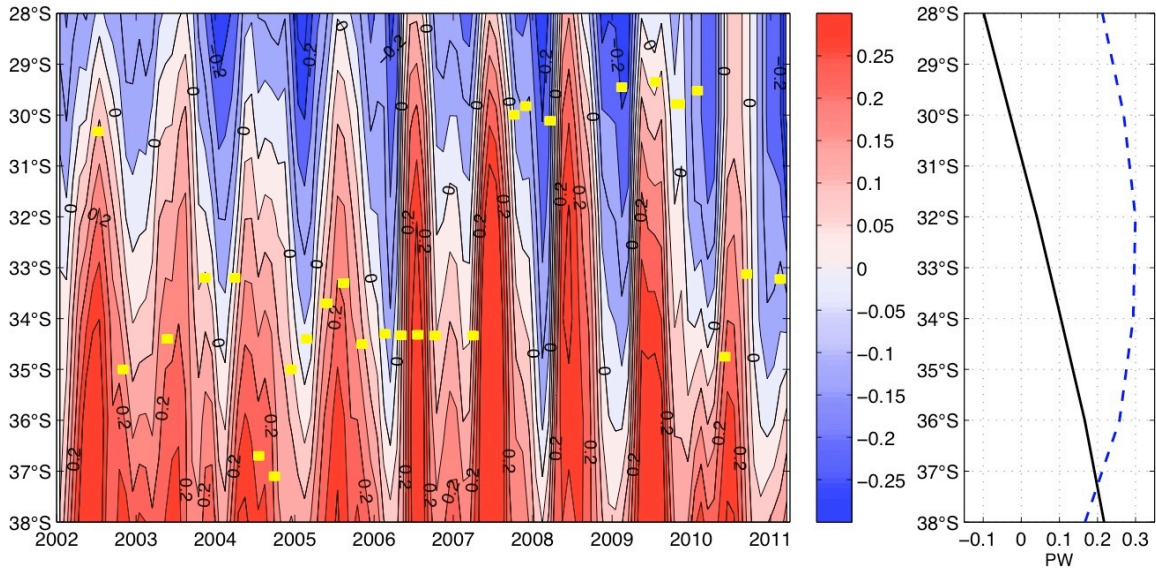


**Figure 2:** (left) Contoured monthly Ekman heat transport in PW derived from daily wind stress values with yellow squares highlighting the time and the mean latitude for the AX18 and AX18\* transects. (right) The mean value of the Ekman heat transport are shown at the right (solid black line) and the amplitude of the seasonal cycle (dashed blue line) as a function of latitude. The Ekman component of the meridional heat flux between 38°S and 28°S was computed using the monthly WOA01 temperatures to determine the mixed layer temperature and NCEP daily wind products.

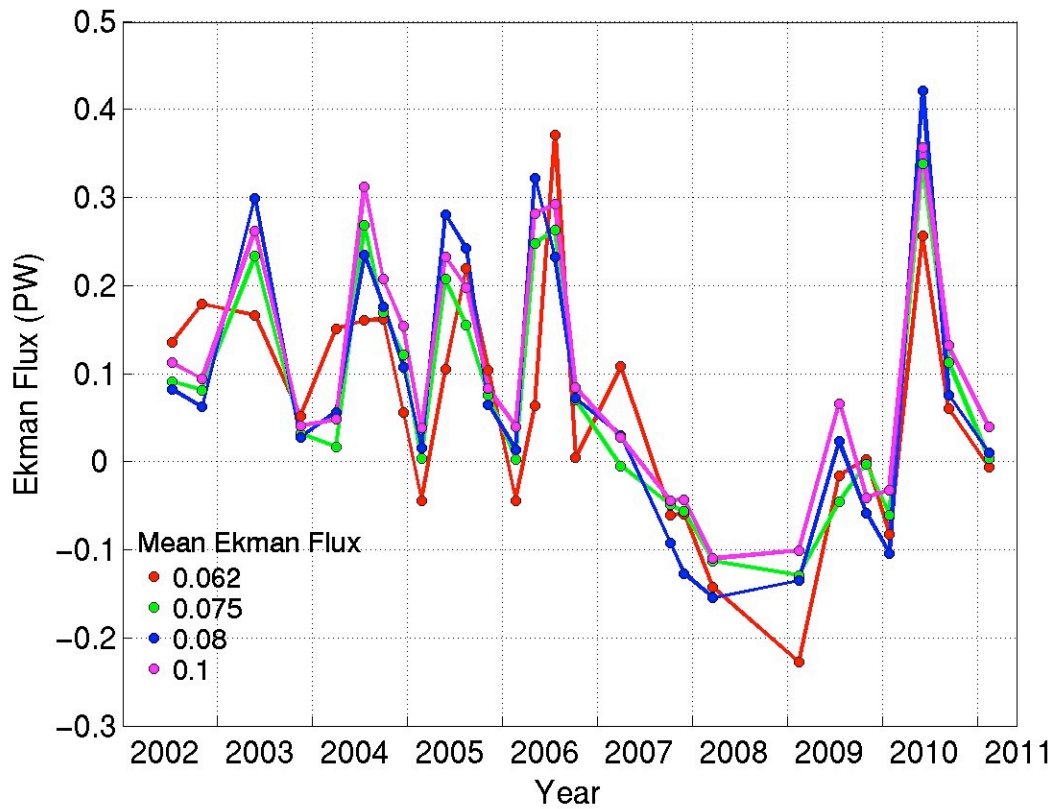


**Figure 3:** Ekman heat transport as a function of time obtained for the following wind products: 1) Hellerman and Rosenstein (1983) monthly winds (blue line), 2) ECMWF monthly winds (pink), 3) NCEP monthly winds (used by Baringer and Garzoli, 2007) (green), and 4) monthly values obtained from the NCEP daily winds (red, this paper) corresponding to the XBT transect dates. Note that the Ekman transport values are computed directly along each XBT section that vary in latitude.

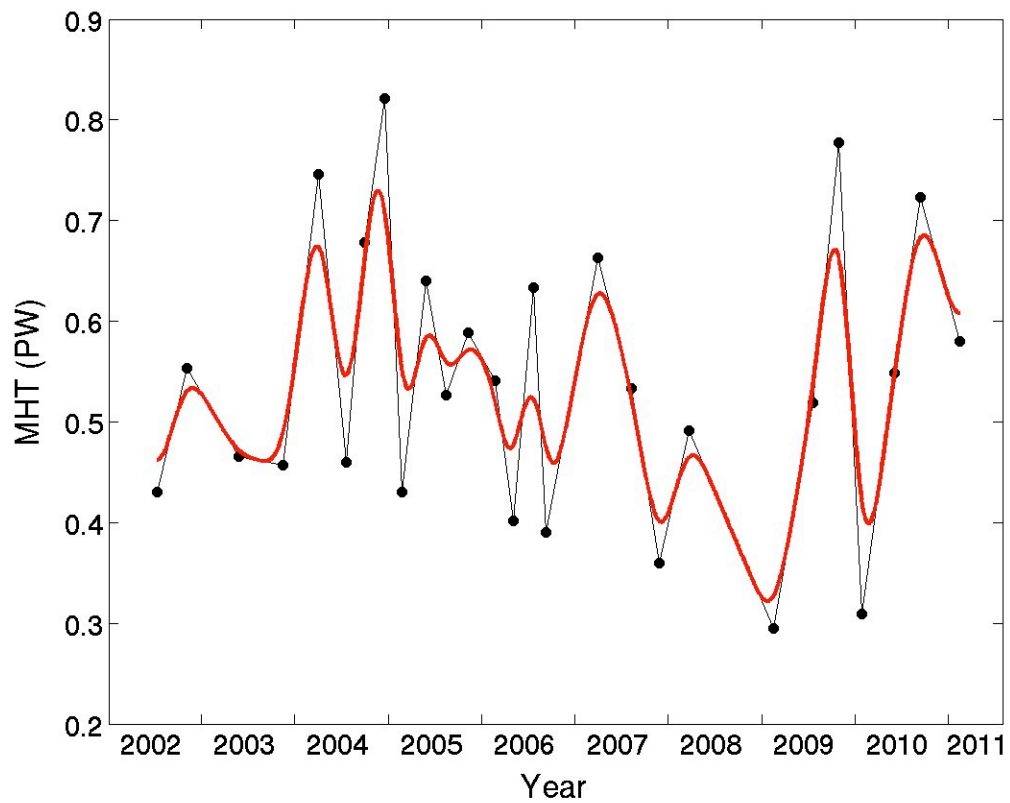


**Figure 4:** Meridional heat transport estimates as a function of time (black dots and line). Superimposed (red curve) is the 183-day running mean of the daily data obtained from linear interpolation of the black curve.

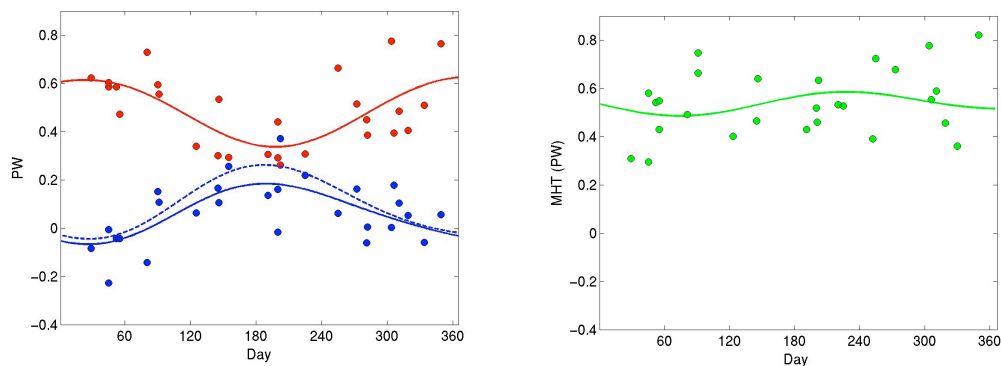


**Figure 5:** Left: Ekman (blue dots) and geostrophic (red dots) components of the MHT estimated from AX18 transects as a function of year-day, with the least-squares fit annual cycle overlaid. The blue dashed line is the annual cycle of the Ekman component of the flux obtained from the original daily NCEP data. Right: Total MHT from AX18 transects as a function of year-day.

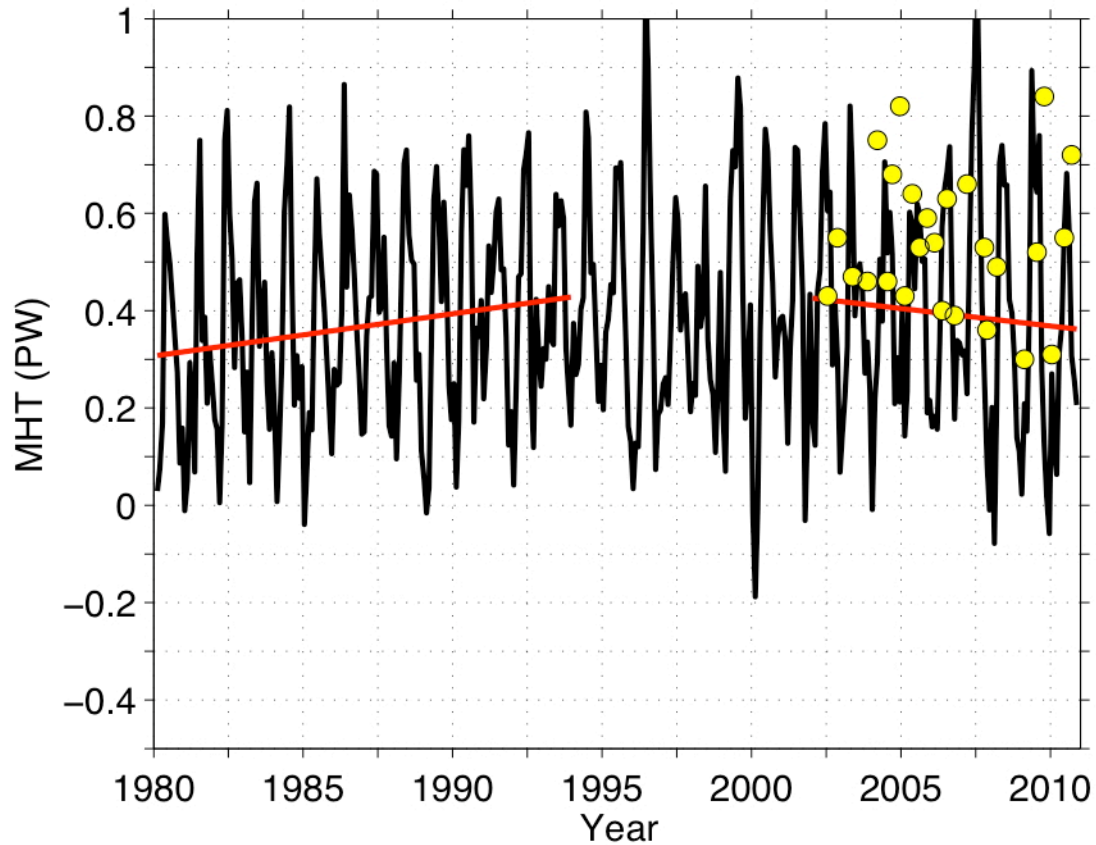


**Figure 6:** MHT along 34.5°S as a function of time estimated from OFES (solid black line) for time scales longer than 60-days. The linear regressions from 1980-1993 and 2002-2010 are shown as red lines. The observed MHT time series along the nominal latitude is overlaid as yellow circles.

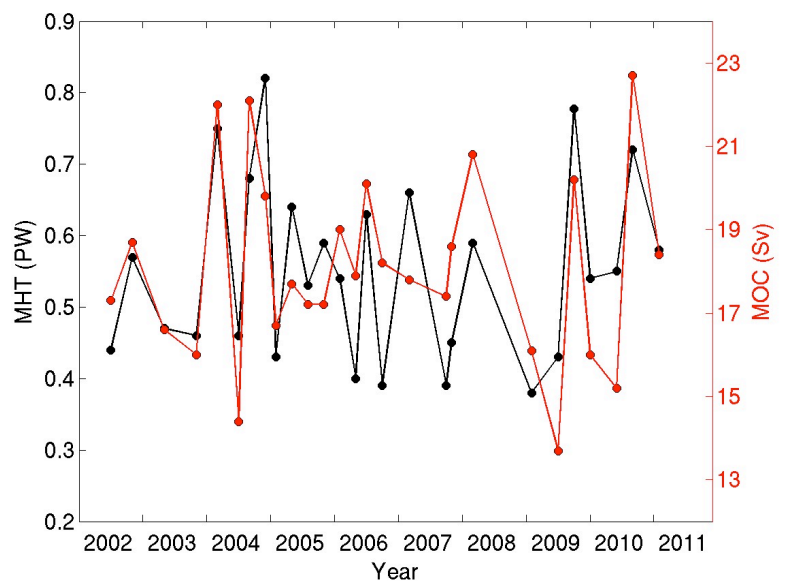


**Figure 7:** Time series of the MHT (black) and the AMOC (red) along nominally 35°S for the time period 2002 to 2011.

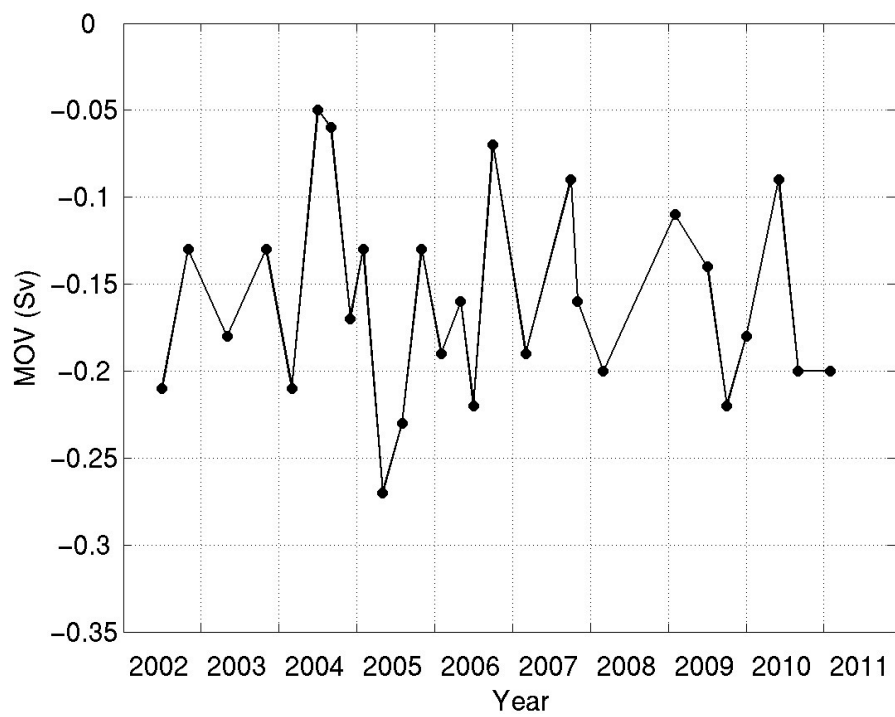


**Figure 8:** Time series of the  $M_{ov}$  nominally across  $35^{\circ}\text{S}$  for the time period 2002 to 2011.

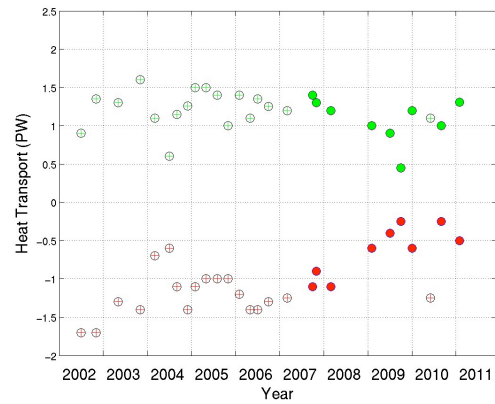
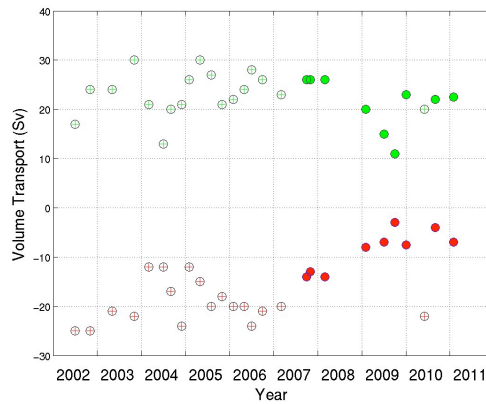


**Figure 9:** Left panel: Volume transport of the Brazil Current at 35°S (red crosses in open circles) and 24°S (red dots) and the volume transport east of 3°E for cruises along 35°S (green crosses in open circles) and those along the diagonal cruises ending near 24°S (green dots). Right panel: the equivalent temperature/heat transports for the Brazil Current and currents east of 3°E.

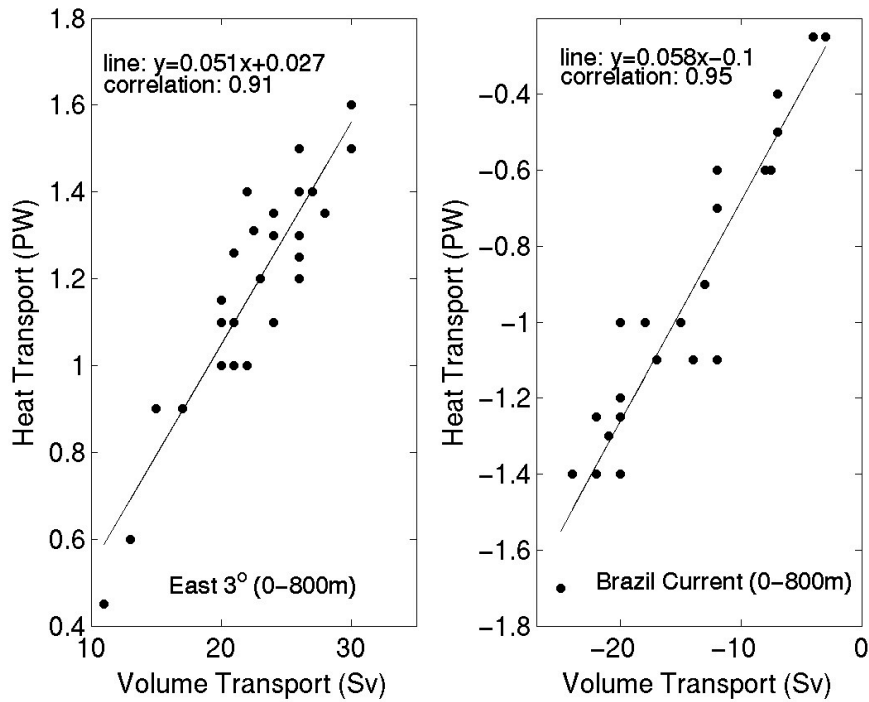
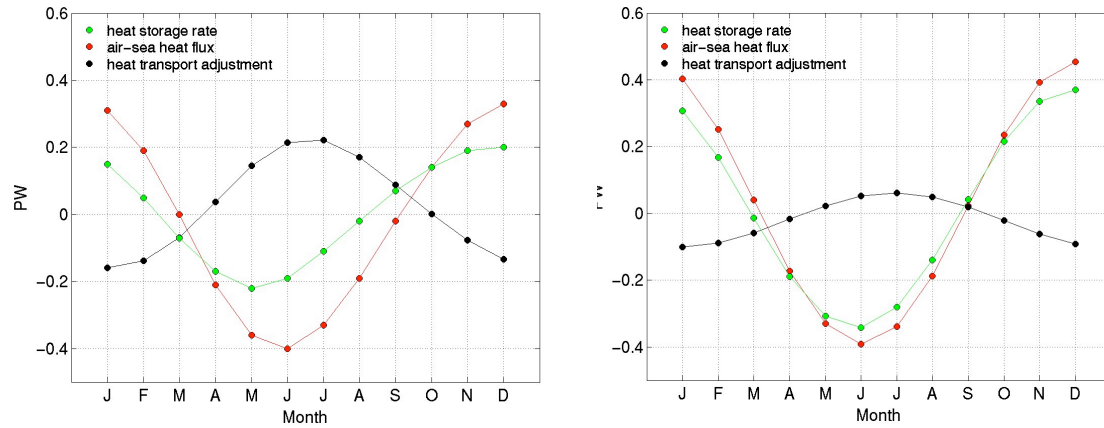


**Figure 10:** Correlation between heat and volume transport for the Brazil Current (left, green dots) and for the flow between 3°E and the African coast (right, red dots) at nominally 35°S. The green and red line is the linear relation between the variables in those two regions, respectively.

990



991

992 **Figure A1:** Heat adjustment from AX18\* transect to AX18 transect obtained as the  
 993 difference between the ocean heat storage rate and the heat gained from the atmosphere  
 994 (within the box highlighted in Fig. 1): Annual cycle of the heat storage rate (green  
 995 circles), air sea heat flux (red circles), and the heat transport adjustment (black circles)  
 996 computed from the observations (left) and OFES (right).

997

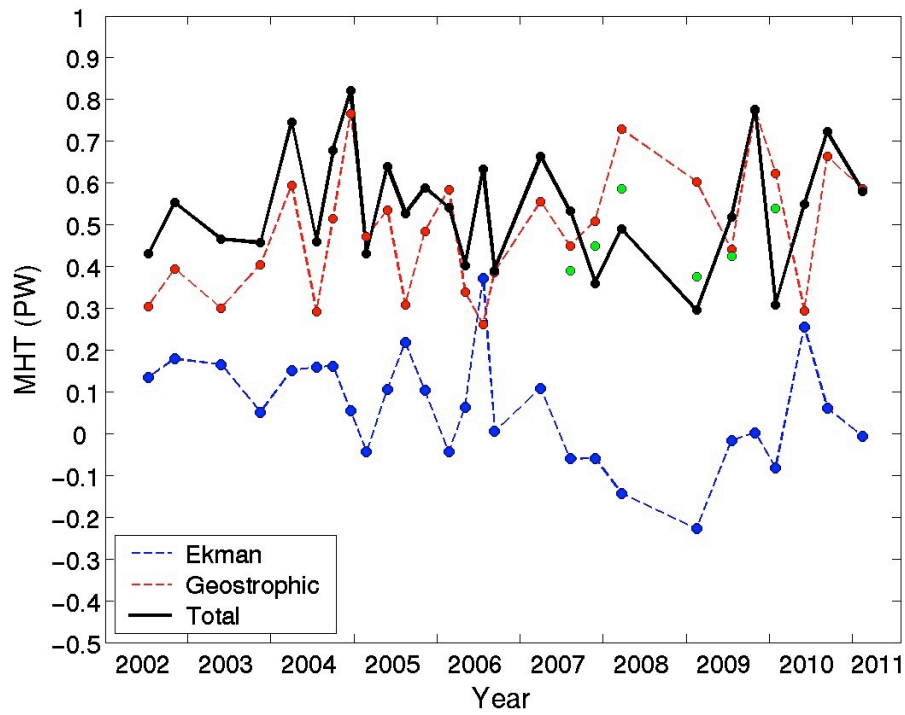


**Figure A2:** MHT as a function of time estimated from AX18 transects (solid black line). The geostrophic and Ekman components of the MHT are shown in red and blue, respectively. Green dots show the unadjusted values collected along AX18\* (see text).